CL-220467 Received: October 27, 2022 | Accepted: November 18, 2022 | Web Released: November 25, 2022

Editor's Choice

Defect Photoluminescence from Alkylated Boron Nitride Nanotubes

Tomohiro Shiraki,*[1,2] Rioe Saito,[1] Hayato Saeki,[1] Naoki Tanaka,[1] Koji Harano,[3] and Tsuyohiko Fujigaya*[1,2,4]

[1]*Department of Applied Chemistry, Graduate School of Engineering, Kyushu University, 744 Motooka, Nishi-ku, Fukuoka 819-0395, Japan*

[2]*International Institute for Carbon-Neutral Energy Research (WPI-I2CNER), Kyushu University, 744 Motooka, Nishi-ku, Fukuoka 819-0395, Japan*

[3]*Research Center for Advanced Measurement and Characterization, National Institute for Materials Science, 1-1 Namiki, Tsukuba, Ibaraki 305-0044, Japan*

[4]*Center for Molecular Systems (CMS), Kyushu University, 744 Motooka, Nishi-ku, Fukuoka 819-0395, Japan*

E-mail: shiraki.tomohiro.992@m.kyushu-u.ac.jp (T. Shiraki), fujigaya.tsuyohiko.948@m.kyushu-u.ac.jp (T. Fujigaya)

Boron nitride nanotubes (BNNTs) are chemically functionalized by a reductive alkylation reaction for defect doping to create luminescent defects. The hexyl group attachment on the BNNT wall results in sp^3 boron atom defect formation in the BN network, by which defect photoluminescence from the functionalized BNNTs is newly observed in a UV–vis region. This chemistry-based defect doping technique offers an attractive tool for bandgap engineering of BNNTs.

Keywords: Boron nitride nanotubes | Defect | Photoluminescence

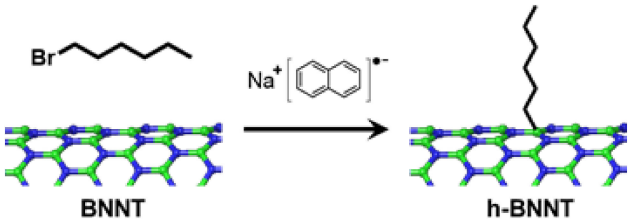

Figure 1. Synthetic scheme for the h-BNNT synthesis. N and B atoms are depicted in blue and green colors, respectively.

Boron nitride nanotubes (BNNTs) are nanocylinders composed of rolled-up hexagonal boron nitride (h-BN) sheets, which were theoretically predicted in 1994[1,2] and experimentally synthesized in 1995.[3] The BN framework consists of alternately connected boron (B) and nitrogen (N) atoms with sp^2 hybridization, by which a strong covalent bond with an ionic character is formed because of their electronegativity difference. Accordingly, BNNTs exhibit unique properties such as high mechanical strength, thermal stability, and a wide bandgap semiconducting feature.[4] Thus, BNNTs have been utilized for various applications including reinforced materials and thermally conductive composites, and also recently used as a key component for one-dimensional (1-D) van der Waals heterostructure fabrication.[5,6]

Because of the large bandgap (≈6 eV) independent of the BNNT diameter and chirality, BNNTs show optical absorption and emission based on the band edge transition in deep UV regions (around 200 nm) for pristine tubes.[7] The observed optical responses are reported to be strongly influenced by excitonic effects.[8,9] In typical BNNT samples, atomic vacancies are formed in the BN framework structure and are reported to yield longer wavelength photoluminescence (PL) in UV–vis regions.[7] This phenomenon indicates a prospect for PL modulation of BNNTs based on defect engineering approaches. For carbon nanotubes (CNTs), which are structural analogues of BNNTs, chemical functionalization for defect engineering has been developed to produce near-infrared defect PL with longer wavelengths and enhanced quantum yields from the functionalized CNTs (locally functionalized single-walled CNTs: lf-SWCNTs).[10–12] To synthesize the lf-SWCNTs, a small amount of chemical functionalization is applied to dope local sp^3 carbon defects in the sp^2 carbon network of CNTs for the formation of luminescent defects. Chemical functionalization for BNNTs[13] has been conducted to modify their surface properties as an alternative to a physical functionalization method.[14] The covalently attached molecules on the BNNT surfaces allowed solubilization of the mostly insoluble BNNTs in various solvents and enhancement of miscibility with matrices in composite fabrication.[13] In this study (Figure 1), chemical functionalization of BNNTs is newly utilized for defect doping to modulate their optical properties; a reductive alkylation reaction produces alkylated BNNTs that emit defect PL based on sp^3 boron atom defect doping for the luminescent defect formation.

BNNTs were purified by heating at 800 °C in air for 2 h, followed by washing with hot water, by which impurities such as amorphous boron are removed.[15] Scanning electron microscope (SEM) images of purified and unpurified BNNTs are shown in Figures 2a and S1, respectively. For the unpurified BNNTs, one-dimensional (1-D) tube-like structures were observed together with spherical particles (a few hundred nm in diameter). In contrast, for the purified BNNTs, only the 1-D structures were confirmed, indicating removal of the impurity particles. Transmission electron microscopy (TEM) showed that the 1-D structures were multiwalled tubes (the common layer number is double-wall) with a diameter of 2–6 nm, as shown in Figures 2b and S2. The purified BNNTs were used for chemical functionalization experiments.

Reductive alkylation of BNNTs was conducted based on a reported procedure.[16] Specifically, BNNTs were reduced by the

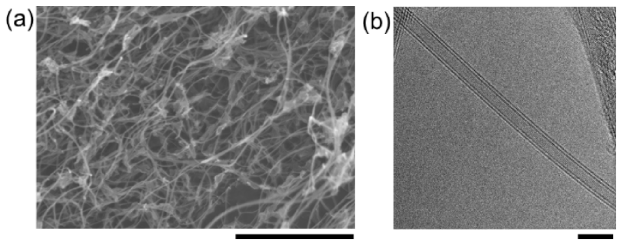

Figure 2. (a) SEM and (b) TEM images of purified BNNTs. Scale bars: 1 µm and 5 nm, respectively.

addition of naphthalene and sodium metal in dry tetrahydrofuran, then mixed with 1-bromohexane. After quenching the reaction, the product was collected by filtration and washed with solvents, providing hexylated BNNTs (h-BNNTs). In the Fourier transform infrared (FT-IR) spectra of h-BNNTs and BNNTs (Figure S3), sharp peaks were observed at ≈790 and ≈1362 cm^{-1}, attributed to the out-of-plane B–N–B bending and the in-plane B–N stretching modes, respectively, in the BN framework.[16,17] The latter signal of h-BNNTs was slightly shifted from that of BNNTs (1371 cm^{-1}), indicating partial distortion of the B–N framework by sp^3 boron atom formation.[16] The h-BNNTs showed a distinct peak around 1090 cm^{-1}, attributed to the vibration modes based on B–C bond formation, together with peaks at 2852, 2924, and 2959 cm^{-1}, attributed to the C–H stretching modes of CH_2 and CH_3 groups.[16,17] Because those signals are not observed for BNNTs, the results indicate the alkylation of BNNTs by this reaction.

The X-ray photoelectron spectroscopy (XPS) spectra for B 1s, N 1s, and C 1s orbitals of h-BNNTs and BNNTs are shown in Figure 3, in which peak deconvolution was conducted using GL (mixture of Gauss and Lorentz) functions. In the XPS survey spectra (Figure S4) and the atomic concentration analysis (Table S1), a small carbon signal for BNNTs was detected, indicating the existence of some carbon impurities. In contrast, h-BNNTs showed a distinct C 1s peak in the spectrum and a large increase in the C content, indicating hexyl group modification. Both h-BNNTs and BNNTs showed obvious peaks at 190 and 398 eV in the B 1s and N 1s, respectively, assigned to B–N bonding in the BN framework.[17] Small signals relating to some oxidized species were detected. For h-BNNTs, new peaks appeared at 189 and 284 eV in the B 1s and C 1s, respectively, assigned to B–C bonding. This result shows covalent bond formation between the boron atom in the BNNT and the hexyl group through the reaction based on electrons (from the sodium reductant) localized on the empty p orbitals of boron atoms.[17] Therefore, the reductive alkylation of BNNTs was confirmed through the B–C bond formation, which induced partial hybridization conversion of boron atoms from sp^2 to sp^3 as a role of defect doping to the crystalline BN framework. A TEM image of multiple h-BNNTs shows that the BNNT surfaces are covered with amorphous organic residues (Figure 4a), suggesting that the BNNT surfaces are modified by the hexyl groups. In the TEM observation, we found a sparsely modified region where a single hexyl group covalently bonded to the outer surface of the double-walled BNNTs was observed (Figure 4b), supported by comparison with the molecular model (Figure 4c) and the simulated image (Figure 4d). The TEM image also demonstrates that the alkylation reaction could mostly maintain the tubular BN network structures in the sp^3 boron atom formation process.

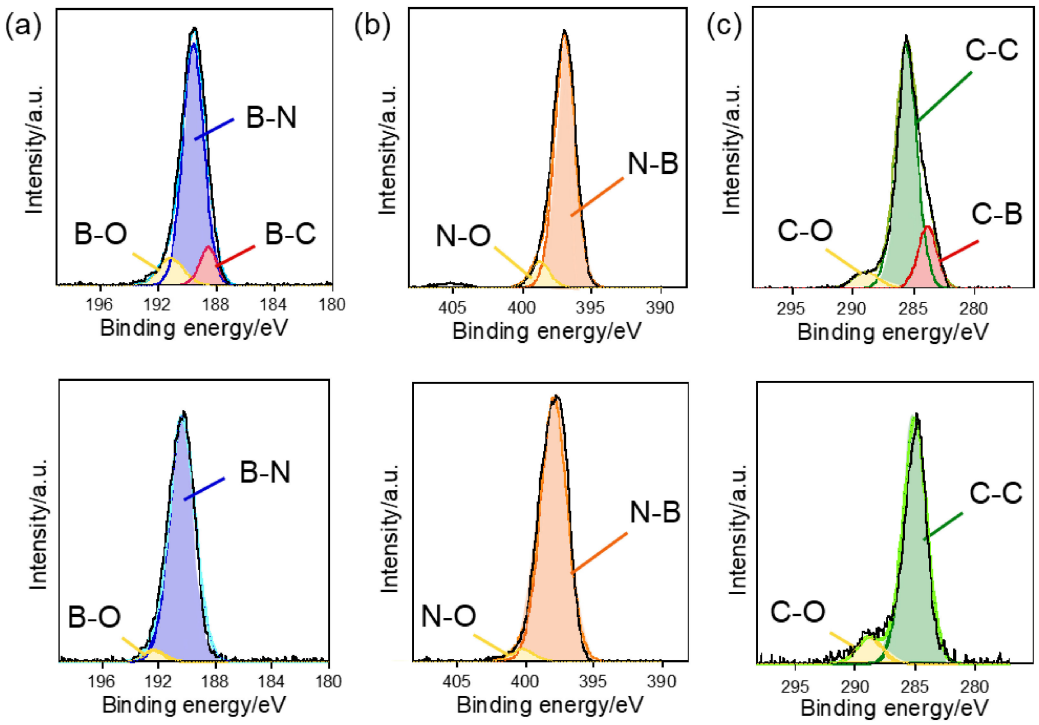

Figure 3. XPS spectra for (a) B 1s, (b) N 1s, and (c) C 1s orbitals of h-BNNTs (upper) and BNNTs (lower). Black and colored lines show measured and deconvoluted spectra, respectively. Peak deconvolution was conducted using GL functions.

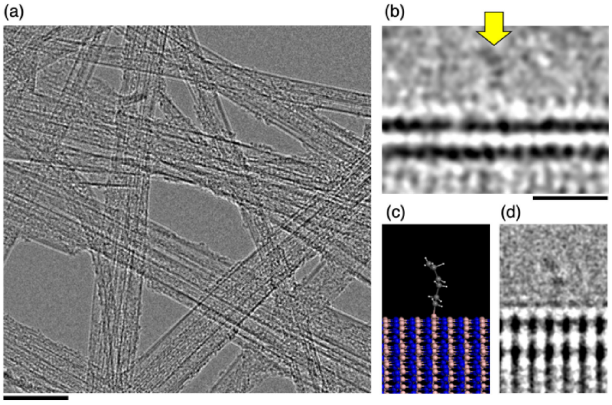

Figure 4. TEM characterization of h-BNNTs. (a) TEM image of h-BNNTs. Scale bar: 20 nm. (b) Atomic-resolution TEM image of a single hexyl chain (indicated by an arrow) attached to a double-walled BNNT. Scale bar: 1 nm. (c) A model of a hexyl group on a double-walled BNNT presented as an atomic-number-correlated molecular model.[18] (d) A corresponding TEM simulation image.

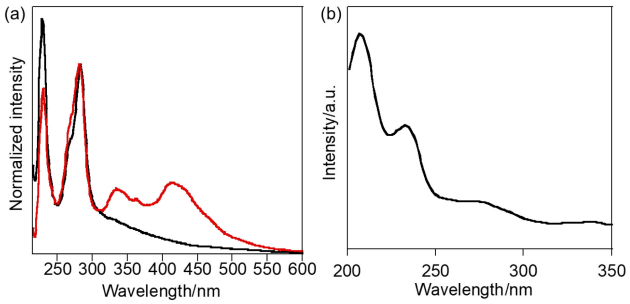

Figure 5. (a) Normalized PL spectra ($\lambda_{ex} = 205$ nm) of BNNTs (black) and h-BNNTs (red) and (b) excitation spectrum ($\lambda_{em} =$ 413 nm) of h-BNNTs in aqueous solutions of 0.020 wt % CTAB.

Thermogravimetric (TG) curves (Figure S5) showed that a weight loss occurred for h-BNNTs around 200–400 °C, although BNNTs exhibited negligible weight changes due to their great thermal stability.[4] Based on the observed weight loss for h-BNNTs, the amount of modified hexyl groups was estimated to be 13.5 wt %, corresponding to one hexyl chain per 22 B–N units in the BN framework.

The spectroscopic analyses were conducted using BNNT and h-BNNT solutions, which were prepared using an aqueous solution of cetyltrimethylammonium bromide (CTAB). In the UV–vis absorption measurements (Figure S6), BNNTs and h-BNNTs showed a clear peak at ≈204 nm, attributed to a bandgap transition of BNNTs.[19] For h-BNNTs, the absorbance increased in the region from 208 to 450 nm, exhibiting partial electronic structure variation by the alkylation reaction. In the PL spectra (Figure 5a), h-BNNTs and BNNTs exhibited PL peaks at 228 nm, assignable to the near bandgap excitonic states and/or quasi donor–acceptor pair emission and free bound transitions, and 282 nm, assignable to the atomic vacancies or impurities (carbon or oxygen).[7,20] Characteristically, h-BNNTs emitted new PL at 334 and 413 nm. In an excitation spectrum for 413 nm PL of h-BNNTs (Figure 5b), not only the bandgap transition (207 nm) but also lower energy absorption bands (233 and 275 nm) contributed to the 413 nm PL, which were similarly observed in the 334 nm PL (Figure S7). These results suggest that the alkylation creates some energy levels in the intrinsically wide bandgap of BNNTs (Figure S8), and photogenerated excitons would migrate in the 1-D tubes and be partially trapped at the defects with the lower energy levels for the defect PL emission, resembling phenomena observed in lf-SWCNTs.[10–12]

When the amounts of chemical reagents were increased by five times for the BNNT alkylation, the amount of the attached alkyl group increased based on a TG result showing 19.5 wt % loss by the alkyl group degradation. However, the defect PL intensity at 413 nm decreased (Figure S9), possibly indicating that the chemical reaction condition could be an important control factor to create luminescent defects in the BN framework.

To date, chemical reactions to change the electronic structures of BNNTs have been rarely reported; Zhi et al. used an amidation reaction using acyl chlorides for amino group anchors possibly introduced in BNNT sidewalls and open ends through a synthetic process of chemical vapor deposition using NH_3 gas, and observed optical property changes explained by a proposed charge transfer-driven doping effect.[19,21] In this study, we use the reductive alkylation for chemical modification of the inherent BN framework and, directly and partly convert the orbital hybridization of the boron atoms from sp^2 to sp^3 as a means of defect doping, which offers a new way to create luminescent defects in BNNTs.

In conclusion, the reductive alkylation of BNNTs newly produced defect PL at 334 and 413 nm in h-BNNTs. Spectroscopic measurements, thermal analysis, and TEM observations confirmed the alkyl group functionalization, in which the B–C bond selectively formed to produce sp^3 boron atom defects in the BN framework for the luminescent defect formation. Consequently, the defect doping functionalization generated new absorption and emission bands. This is the first report of a luminescent defect formation in BNNTs based on defect doping by atomic orbital hybridization conversion using a chemical functionalization technique. Chemical functionalization would enable the versatile design of molecular structures of the defect-doped sites in the functionalized BNNTs, which would offer novel band engineering techniques of BNNTs and produce a wide variety of molecularly functionalized BNNTs for advanced optical applications such as single-photon emitters in quantum technologies.

We thank Dr. Koji Kimoto (National Institute for Materials Science) for assistance with the TEM observations. This study was supported by Grants-in-Aid, the Groundbreaking Research Project from the Faculty of Engineering of Kyushu University, the JSPS KAKENHI (Grant Numbers JP22H01910 and JP21H01758), and the Nanotechnology Platform Project, from the Ministry of Education, Culture, Sports, Science and Technology, Japan.

Supporting Information is available on https://doi.org/10.1246/cl.220467.

References

1 A. Rubio, J. L. Corkill, M. L. Cohen, *Phys. Rev. B* **1994**, *49*, 5081.

2 X. Blase, A. Rubio, S. G. Louie, M. L. Cohen, *Europhys. Lett.* **1994**, *28*, 335.
3 N. G. Chopra, R. J. Luyken, K. Cherrey, V. H. Crespi, M. L. Cohen, S. G. Louie, A. Zettl, *Science* **1995**, *269*, 966.
4 D. Golberg, Y. Bando, Y. Huang, T. Terao, M. Mitome, C. Tang, C. Zhi, *ACS Nano* **2010**, *4*, 2979.
5 R. Xiang, T. Inoue, Y. Zheng, A. Kumamoto, Y. Qian, Y. Sato, M. Liu, D. Tang, D. Gokhale, J. Guo, K. Hisama, S. Yotsumoto, T. Ogamoto, H. Arai, Y. Kobayashi, H. Zhang, B. Hou, A. Anisimov, M. Maruyama, Y. Miyata, S. Okada, S. Chiashi, Y. Li, J. Kong, E. I. Kauppinen, Y. Ikuhara, K. Suenaga, S. Maruyama, *Science* **2020**, *367*, 537.
6 S. Furusawa, Y. Nakanishi, Y. Yomogida, Y. Sato, Y. Zheng, T. Tanaka, K. Yanagi, K. Suenaga, S. Maruyama, R. Xiang, Y. Miyata, *ACS Nano* **2022**, *16*, 16636.
7 L. Museur, A. Kanaev, *J. Appl. Phys.* **2015**, *118*, 084305.
8 J. Yu, D. Yu, Y. Chen, H. Chen, M.-Y. Lin, B.-M. Cheng, J. Li, W. Duan, *Chem. Phys. Lett.* **2009**, *476*, 240.
9 C.-H. Park, C. D. Spataru, S. G. Louie, *Phys. Rev. Lett.* **2006**, *96*, 126105.
10 T. Shiraki, *Chem. Lett.* **2021**, *50*, 397.
11 T. Shiraki, Y. Miyauchi, K. Matsuda, N. Nakashima, *Acc. Chem. Res.* **2020**, *53*, 1846.
12 A. H. Brozena, M. Kim, L. R. Powell, Y. Wang, *Nat. Rev. Chem.* **2019**, *3*, 375.
13 Q. Weng, X. Wang, X. Wang, Y. Bando, D. Golberg, *Chem. Soc. Rev.* **2016**, *45*, 3989.
14 Z. Gao, K. Fujioka, T. Sawada, C. Zhi, Y. Bando, D. Golberg, M. Aizawa, T. Serizawa, *Polym. J.* **2013**, *45*, 567.
15 H. Chen, Y. Chen, J. Yu, J. S. Williams, *Chem. Phys. Lett.* **2006**, *425*, 315.
16 H. Shin, J. Guan, M. Z. Zgierski, K. S. Kim, C. T. Kingston, B. Simard, *ACS Nano* **2015**, *9*, 12573.
17 C. A. de los Reyes, K. L. W. Mitra, A. D. Smith, S. Yazdi, A. Loredo, F. J. Frankovsky, E. Ringe, M. Pasquali, A. A. Martí, *ACS Appl. Nano Mater.* **2018**, *1*, 2421.
18 J. Xing, K. Takeuchi, K. Kamei, T. Nakamuro, K. Harano, E. Nakamura, *Proc. Natl. Acad. Sci. U.S.A.* **2022**, *119*, e2114432119.
19 C. Zhi, Y. Bando, C. Tang, S. Honda, K. Sato, H. Kuwahara, D. Golberg, *Angew. Chem., Int. Ed.* **2005**, *44*, 7932.
20 A. Pierret, H. Nong, F. Fossard, B. Attal-Trétout, Y. Xue, D. Golberg, J. Barjon, A. Loiseau, *J. Appl. Phys.* **2015**, *118*, 234307.
21 C. Zhi, Y. Bando, C. Tang, D. Golberg, *Phys. Rev. B* **2006**, *74*, 153413.

